Nonequilibrium interband phase textures induced by vortex splitting in two-band superconductors

A. S. Mosquera Polo,[1,2] R. M. da Silva,[1] A. Vagov,[3] A. A. Shanenko,[1] C. E. Deluque Toro,[2] and J. Albino Aguiar[1,*]

[1]*Departamento de Física, Universidade Federal de Pernambuco, Av. Jorn. Aníbal Fernandes, s/n, Cidade Universitária, 50740-560 Recife-PE, Brazil*

[2]*Grupo de Nuevos Materiales, Facultad de Ingenieria, Universidad del Magdalena, Carrera 32 No 22-08, Santa Marta, Colombia*

[3]*Department of Physics, Bayreuth University, Bayreuth 95440, Germany*

(Received 25 April 2017; revised manuscript received 7 July 2017; published 21 August 2017)

We demonstrate that in a weak-coupled two-band superconducting slab the interaction between vortices penetrating the sample and its boundaries leads to the phenomenon of vortex splitting, which divides composite vortices and creates fractional ones. The interaction between vortices, attractive for different bands and repulsive for the same band, which is controlled by the electric current density flowing through the system, leads to an ordered alternating arrangement of the vortices. This arrangement creates nonequilibrium interband phase textures or domains with different signs of the Josephson energy of the interaction between the band condensates. Such phase textures have a significant effect on the dissipation caused by the vortex motion. In particular, in the phase-texture regime the onset of the dissipation is shifted to higher current densities.

DOI: 10.1103/PhysRevB.96.054517

I. INTRODUCTION

Appearance of multiple different Cooper pairing channels for different bands in a single superconductor gives rise to the phenomenon of multiband superconductivity, where multiple gaps (condensates) give rise to additional degrees of freedom of the superconducting state. For materials with two bands with the singlet s-wave pairing, such as MgB_2, one of those degrees of freedom is the difference between phases of the band gap condensates. The phase difference manifests itself, in particular, in the sign of the linear (Josephson) coupling between the bands, which determines the interaction between the band condensates. The degree of freedom related to the phase difference can be excited (driven out of equilibrium) by an external force. Such excitations in systems with many condensates are commonly referred to as the Leggett modes [1]. Theoretical studies of their properties have intensified after discovering the multiband superconductivity in materials such as MgB_2 [2], iron pnictides [3,4], and others [5]. Experimental evidences of the Leggett modes has been published recently [6].

Nonequilibrium configurations of the phase difference between the gap functions can be remarkably nontrivial. For example, in superconductors with three or more bands one has a possibility to achieve a ground state with a broken time-reversal symmetry (BTRS) [7]. Such states are characterized by fixed differences between the band condensate phases being at the same time degenerate. In spatially extended samples this degeneracy can lead to inhomogeneous configurations of the condensate, where domains of different degenerate states alternate, being separated by the domain walls [8,9]. Theoretical studies of formation, stabilization, and detection of such domain walls have been recently reported [10–12]. In quasi-one-dimensional (1D) samples topological solitons or phase textures can appear [13–15], with a 1D structure of domain walls. These states are nonequilibrium and are induced by imbalanced carriers due to an injected current. To this date such configurations, however, have not been confirmed experimentally.

Elementary entities, serving as building blocks for all nontrivial phase configurations in 2D structures, are vortices. Multiband superconductors can develop vortex states that are qualitatively different from those in single-band materials. A trivial configuration is a composite vortex that comprises two vortices in the band condensate, that are centered at the same point, and have equal winding numbers. Stationary equilibrium states in two-band bulk superconductors are formed by the composite vortices. However, a nonequilibrium system can develop a state with the band vortices that are shifted spatially, the so-called noncomposite vortices. Those vortices are associated with a nonquantized magnetic flux: each of the partial vortices in the band condensates carry a fraction of the total (quantized) flux, and are often called fractional vortices.

In bulk superconductors fractional vortex states cannot exist due to a divergent energy [16]. However, in samples of finite dimensions metastable fractional vortices can appear [17–21]. One of the mechanism which creates noncomposite fractional vortices is the dynamical vortex dissociation. This mechanism appears, for example, when a superconductive current flows through the sample. In this case differences in the driving forces and the viscosity of the vortex matter in each of the condensates drive the band vortices apart [22].

At certain conditions a multiband superconductor can reveal domains of different phase structures with quasi-1D walls between them. Appearance of such domain walls, excited dynamically between regions of contrasting phase difference and decorated by moving vortex sheets, have been predicted for p-wave multiband superconductors [23]. However, in two-band s-wave superconductors the phase textures has been predicted theoretically only for quasi-1D structures, where they are induced by imbalances in the normal current through the contact interfaces at the sample ends [13,14].

In this work we describe another mechanism that induces topological phase textures in a weak-coupled two-band superconductor with the s-wave pairing. Contrary to the earlier

*Corresponding author: albino@df.ufpe.br

works [13,14] it produces quasi-1D domains in 2D samples of finite dimensions when a superconductor with a flowing current is placed in a constant magnetic field. We demonstrate that in such systems a nonequilibrium vortex matter is created, forming domains of shifted phases of the band condensates. A key ingredient of this mechanism is the dynamical vortex splitting, where vortices become fractional. This mechanism does not depend on the special contacts at the ends of the sample and in principle can be found in any weak-coupled multiband material.

Our analysis is done for a two-band prototype model described by the two-component time-dependent Ginzburg-Landau (TCGL) equations. The difference between the band condensate phases is characterized by the Josephson energy that enters the free energy functional of the system. A nonequilibrium vortex matter is created by the applied magnetic field in a combination with the flowing current. The nonequilibrium vortex dynamics results in the energy loss, which in turn leads to a finite resistance of the system, reflected in the current-voltage (I-V) characteristics.

In the paper, Sec. II describes the model and its numerical solution. Results of the calculations showing different development stages of the vortex matter types are discussed in Sec. III B. The relation between the phase textures and the resistance is described in Sec. III C. Section III D is devoted to the role of the size effects. Summary of the results are given in Sec. IV.

II. MODEL AND METHOD

The Gibbs energy functional of the TCGL model is defined by its energy density [24–26]

$$g = \frac{(\mathbf{B}-\mathbf{B}_0)^2}{8\pi} + \sum_{j=1,2}\left\{\frac{1}{2m_j}|\mathbf{D}\psi_j|^2 + \alpha_j|\psi_j|^2 + \frac{1}{2}\beta_j|\psi_j|^4\right\} + g_J, \quad g_J = -\Gamma(\psi_1^*\psi_2 + \psi_1\psi_2^*), \quad (1)$$

where $\psi_1 = |\psi_1|\exp(i\theta_1)$ and $\psi_2 = |\psi_2|\exp(i\theta_2)$ are complex gap (condensate) functions of the bands $j = 1,2$, $\mathbf{D} = -\mathbb{i}\hbar\nabla - 2e\mathbf{A}/c$ is the gauge-invariant gradient, $\mathbf{B} = [\nabla \times \mathbf{A}]$ is the magnetic field, $\mathbf{B}_0$ is the applied (external) field, g_J is the interband coupling or the Josephson energy, α_j, β_j, m_j are material constants defined as

$$\alpha_j = -N(0)n_j\chi_j, \quad \beta_j = N(0)\frac{n_j}{W^2}, \quad m_j = \frac{3W^2}{N(0)n_j v_j^2}, \quad \Gamma = N(0)\frac{\lambda_{12}}{G}, \quad W^2 = \frac{8\pi^2 T_c^2}{7\zeta(3)}, \quad \chi_j = \tau - \frac{S_j}{n_j G}, \quad (2)$$

where $\tau = 1 - T/T_c$, $N_j = N(0)n_j$ is the band density of states (DOS) at the Fermi energy, $N(0) = N_1 + N_2$ is the total DOS ($n_1 + n_2 = 1$), $\lambda_{ij} = g_{ij}N(0)$ are dimensionless coupling constants for the coupling constants g_{ij}, $G = \lambda_{11}\lambda_{22} - \lambda_{12}^2$, v_j is the band Fermi velocity, and S_1, S_2 appears in the solution of the linearized gap equation for the critical temperature T_c and are defined similar to the earlier works [27]

$$S_1 = \lambda_{22} - n_1 GS, \quad S_1 = \lambda_{11} - n_2 GS,$$
$$S = \frac{n_1\lambda_{11} + n_2\lambda_{22} \pm \sqrt{(n_1\lambda_{11} + n_2\lambda_{22})^2 + 4n_1n_2\lambda_{12}^2}}{2n_1n_2G}. \quad (3)$$

The time-dependent TCGL equations are found from the stationary condition of the energy functional with the additional dynamical contributions, this yields

$$\eta_1\frac{\partial\psi_1}{\partial t} = \frac{1}{2m_1}\mathbf{D}^2\psi_1 + \alpha_1\psi_1 + \beta_1|\psi_1|^2\psi_1 - \Gamma\psi_2,$$
$$\eta_2\frac{\partial\psi_2}{\partial t} = \frac{1}{2m_2}\mathbf{D}^2\psi_2 + \alpha_2\psi_2 + \beta_2|\psi_2|^2\psi_2 - \Gamma\psi_1, \quad (4)$$

where we introduce the relaxation constants η_j for the respective bands. The accompanying Maxwell equation writes as

$$\frac{c}{4\pi}[\nabla \times [\nabla \times \mathbf{A}]] = \mathbf{J}_n + \mathbf{J}_s, \quad (5)$$

where $\mathbf{J}_s$ is the supercurrent

$$\mathbf{J}_s = 2e\mathrm{Re}\left[\frac{1}{m_1}\psi_1\mathbf{D}^*\psi_1^* + \frac{1}{m_2}\psi_2\mathbf{D}^*\psi_2^*\right], \quad (6)$$

and $\mathbf{J}_n$ is the normal current induced by the electric field

$$\mathbf{J}_n = \sigma\mathbf{E} = -\frac{\sigma}{c}\frac{\partial\mathbf{A}}{\partial t}, \quad (7)$$

with σ being the normal conductivity of the material.

Although characteristic lengths of this model strongly depend on the coupling between the bands, one can still define the coherence and the penetration lengths for each band, considered separately, by using the standard GL expressions

$$\xi_j = \frac{\hbar v_j}{\sqrt{6}W}, \quad \lambda_j = \sqrt{\frac{3c^2}{16\pi N(0)e^2 n_j v_j^2}}. \quad (8)$$

One can also define the GL parameter κ for each of the bands as

$$\kappa_j = \frac{\lambda_j}{\xi_j}, \quad \frac{\kappa_2}{\kappa_1} = \sqrt{\frac{n_1}{n_2}}\frac{v_1^2}{v_2^2}. \quad (9)$$

For a single-band superconductor the GL parameter determines a superconductivity type of an uncoupled band, so that when $\kappa_j < 1/\sqrt{2}$ the band is a type-I and if $\kappa_j > 1/\sqrt{2}$ the band is a type-II superconductor.

The material parameters are taken as $\lambda_{11} = 2.0$, $\lambda_{22} = 1.03$, $\lambda_{12} = 10^{-4}$, $\alpha = v_1/v_2 = 0.52$, $\kappa_1 = 10.0$, $n_1 = 0.355$. Despite this choice does not correspond to any particular material, it addresses the general case in which there is a discrepancy between the vortex sizes in different bands.

Using these parameters one can calculate the critical temperature T_c of the superconductor as well as the critical temperatures T_{cj} for each of the bands, taken separately, which is found from equations $\alpha_j = 0$,

$$T_{cj} = T_c\left(1 - \frac{S_j}{n_j G}\right), \quad (10)$$

which for the chosen microscopic parameters yields $T_{c1} = 0.9997\,T_c$ and $T_{c2} = 0.9030\,T_c$. We set $T = 0.85T_c$ in our

calculations which is sufficiently close to T_c but is lower than both T_{c1} and T_{c2}, so that both superconducting bands are active.

For the chosen parameters one obtains $\kappa_1 = 10.0$ and $\kappa_2 = 2.0$, i.e., both bands (separately) are type-II superconductors. The ratio of the band coherence lengths is found as $\xi_2/\xi_1 = 2.24$. Following the standard terminology we refer to the band $j = 1$ as "strong" and to the band $j = 2$ as "weak." The flux quantum Φ_0 can be divided into two fractional parts which are approximately given by the expression $\phi_j = \lambda^2\Phi_0/\lambda_j^2$ taken from the London limit [22]. In this way, $\phi_1 = 0.72\Phi_0$ and $\phi_2 = 0.28\Phi_0$, for the magnetic flux carried in the first and second band by a single vortex state.

For the numerical calculations it is convenient to scale all relevant quantities using parameters of the stronger band $j = 1$,

$$\psi_j = W\tilde{\psi}_j, \quad \mathbf{r} = \xi_1\tilde{\mathbf{r}}, \quad \mathbf{A} = A_0\tilde{\mathbf{A}},$$
$$t = t_0\tilde{t}, \quad \eta_j = \eta_0^j\tilde{\eta}_j, \tag{11}$$

where

$$A_0 = \frac{\hbar c}{2e\xi_1}, \quad t_0 = \frac{4\pi\sigma\kappa_1^2\xi_1^2}{c^2}, \quad \eta_0^j = n_j N(0) t_0. \tag{12}$$

The scaled TCGL equations read as (hereafter we omit "tilde" for the scaled quantities)

$$\eta_1\frac{\partial\psi_1}{\partial t} = \mathbf{D}^2\psi_1 - (\chi_1 - |\psi_1|^2)\psi_1 - \gamma\psi_2,$$
$$\eta_2\frac{\partial\psi_2}{\partial t} = \frac{1}{\alpha}\mathbf{D}^2\psi_2 - (\chi_2 - |\psi_2|^2)\psi_2 - \gamma\frac{n_1}{n_2}\psi_1, \tag{13}$$

where the gradient-invariant derivative is $\mathbf{D} = -i\nabla - \mathbf{A}$, $\gamma = \lambda_{12}/(n_1 G)$ and for the decay rates we assume $\eta_1 = \eta_2 = 5.0$. Equation (5) becomes

$$\frac{\partial \boldsymbol{A}}{\partial t} = \mathrm{Re}\left[\psi_1\mathbf{D}^*\psi_1^* + \frac{1}{\alpha}\frac{n_2}{n_1}\psi_2\mathbf{D}^*\psi_2^*\right] - \kappa_1^2[\nabla\times[\nabla\times\boldsymbol{A}]]. \tag{14}$$

We consider a sample of the form of an infinite rectangular slab with cross-section dimensions $L \times w$. By choosing a slab of infinite length we neglect the demagnetization effects, thereby restricting the effective dimensionality of the system to 2D. Equations (13) and (14) are solved with the periodic boundary conditions along the x direction ($L = 600\xi_1$) and the standard GL condition

$$\mathbf{D}_y\psi_j = 0 \tag{15}$$

in the y direction, where the vector component y is perpendicular to the surface of the sample. The numerical solution is performed on a two-dimensional square grid with spacings $a_x = a_y = \xi_1$ using the $U-\Psi$ method [28,29] combined with the parallelized Euler finite difference algorithm for the time evolution.

The vortex dynamics is induced by applying an external current with the density $\mathbf{j}$ flowing through the sample in $\mathbf{x}$ direction. In the numerical calculations the current is modeled by introducing an additional magnetic field $\Delta\mathbf{B}$, related to $\mathbf{j}$ by Eq. (5). In the chosen geometry this extra field is directed along the z axis and is constructed so that the total magnitude of the applied field is $B = B_0 - \Delta B$ at $y = 0$ and $B = B_0 + \Delta B$ at $y = w$. Taking into account that $\mathbf{B} = [\nabla\times\boldsymbol{A}]$ together with Eq. (5) one obtains the value of the current density as $j = c\Delta B/2\pi$.

Nontrivial phase configurations are typically associated with the appearance of elementary topological structures such as vortices, domains walls, etc. Here we are interested in the phase configurations specific to two-band systems, in particular, we investigate a phase difference between the band condensates $\Delta\theta = \theta_1 - \theta_2$. A natural parameter that characterizes such two-band phase differences is the Josephson energy $g_J = -2\gamma|\psi_1||\psi_2|\cos(\Delta\theta)$, which describes the intercondensate interaction and was also used to investigate topological solitons of alternating phases in quasi-1D samples of two-band superconductors [14].

We also note that the phase dynamics is necessarily associated with the energy losses, which lead to the finite resistivity of the system. In our case this will be detected from the appearance of a finite potential or voltage across the sample in x direction for a given value of the current j (the I-V curve). The current density is measured in the units of j_0, which is the critical current density for the sample geometry and microscopic parameters introduced in this section. The unit for the voltage across the sample is $V_0 = V(j_0)$.

III. RESULTS

A. Vortices near sample boundaries, general picture

Before presenting results of the numerical calculations we recall that unlike quasi-1D systems, where domain walls (solitons) form nontrivial phase structures, in 2D infinite samples vortices are such elementary building blocks that construct nontrivial topological structures. As mentioned above in infinite equilibrium two-band systems only composite vortices can exist, where vortices in each band share the same center point and have the same winding number. This is a manifestation of the attraction between vortices in different bands, that is referred for simplicity to as the interband attraction.

However, in finite samples vortices also interact with the boundaries and this strongly affects vortex states. One notes that vortices enter a superconducting sample through its boundaries. The manifestation of this interaction is the so-called Bean-Livingston (BL) barrier [30] which delays the process of vortex penetration. The delay depends on the size of the vortex core, determined by the coherence length ξ, and is different for different bands in a multiband system [20,21].

In our two-band case the effective BL barrier is higher for vortices in the strong band and vortices of this band tend to remain longer in the vicinity of the boundary. On the contrary, vortices in the weak band penetrate the BL barrier faster. Obviously this difference is more pronounced for materials with a considerable discrepancy between the characteristic lengths ξ_1 and ξ_2. The difference in the penetration time leads to dynamical separation or "dissociation" of composite vortices and thereby to creation of fractional vortices. This in turn leads to the appearance of domains of $g_J > 0$, located between separated vortices. An appearance of such noncomposite or fractional vortices near the boundary can be in principle detected experimentally [21].

For isolated vortices their interaction with the surface is restricted to the layer of width $l \sim \lambda$ near the boundary. Once fractional vortices move outside this layer, the influence of the surface diminishes and vortices tend to become composite again (recombination) due to the attractive interaction of the vortices in different bands (interband attraction). However, this changes for a dense vortex matter. In this case the vortex matter is strongly influenced by the interaction between vortices, in particular, due to the additional repulsion between vortices in the same band (intraband repulsion). This may lead to appearance of dynamically unstable but long-lived vortex configurations, with nontrivial spatial distribution of the interband phase difference.

B. Vortex splitting and phase textures, numerical results

Numerical calculations of the TCGL equations are done for a sample in the form of a slab with a rectangular cross section with dimensions $L = 600\xi_1$ and $w = 150\xi_1$. The slab is placed in the magnetic field parallel to the z axis, i.e., along the slab (assumed infinite in this direction to exclude the demagnetization effects). The magnetic field $H = 0.73H_c$ is chosen to be larger than the lower critical field of the material $H > H_{c1}$.

As discussed above, the electric current with the density $\mathbf{j} = (j,0,0)$ facilitates penetration of the magnetic field inside the sample. Initial configuration is taken as a random distribution of the band-condensate densities with a small amplitude. The value of the initial magnetic field exceeds H_{c1}, and therefore vortices are present in the sample already at $j = 0$. This vortex state remains stationary if the current is sufficiently small. However, when j exceeds the threshold $0.23\,j_0$ vortices start to move from the upper boundary $y = w$, which is their entry point, to the lower one, the exit point at $y = 0$. Furthermore, penetrating vortices are not composite and create domains of positive Josephson energy.

This is illustrated in Fig. 1, which shows snapshots of spatial distributions of g_J, taken at certain time instants, as the color density plot. Figures 1(a)–1(e) correspond to few selected values of the applied current density $j = 0.33,0.37,0.47,0.57,0.77\,j_0$. Areas with $g_J < 0$ and $g_J > 0$ are marked, respectively, red and blue.

Figure 1(a) with $j = 0.33\,j_0$ represents a situation when the current is only slightly above the threshold. Vortices inside the sample are composite and arranged in the lattice. Still, in the vicinity of the surface fractional vortices appear with small areas of shifted band phases with $g_J > 0$.

When the current increases, fractional vortices start to penetrate deeper inside the sample, forming larger domains of $g_J > 0$. This is illustrated in Fig. 1(b), calculated for $j = 0.37\,j_0$. Domains with $g_j > 0$ grow with the current. Eventually they reach the lower boundary, as is shown in Fig. 1(c), calculated for $j = 0.47\,j_0$. When the current further increases, domains of $g_J > 0$ straighten, forming perpendicular textures [cf. Fig. 1(d) calculated for $j = 0.57\,j_0$], similar to solitons observed in quasi-1D systems [14]. Notice that the phase textures are not static. They change with time, especially in the lower parts of the larger textures, where the vortices exit the sample. The time evolution persists until straight channel-like textures connect the upper and the lower edges

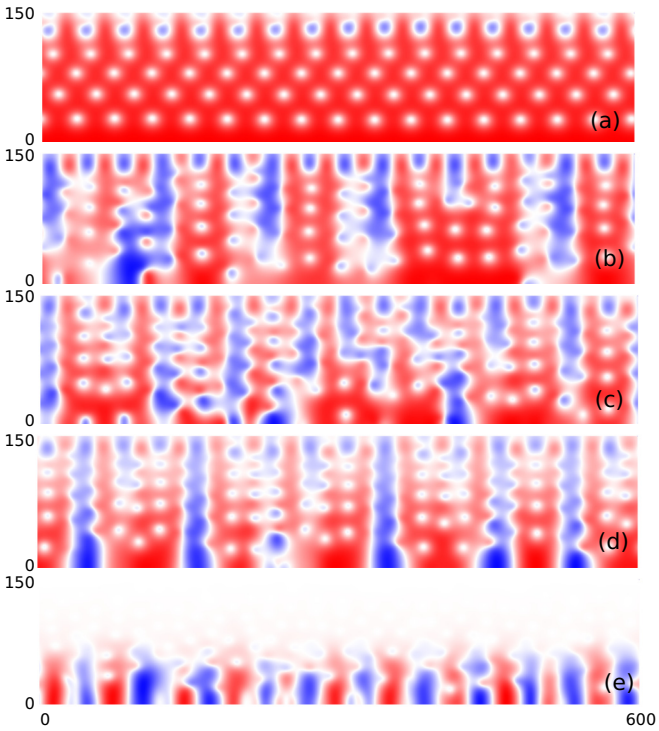

FIG. 1. Snapshots of the spatial distribution of the Josephson energy g_J, plotted as color density plots, as defined in Eq. (1), calculated for the slab with the cross section 600×150 (in the ξ_1 units). Domains of $g_J < 0$ and $g_J > 0$ are marked by red and blue, respectively, color intensity gives the absolute value $|g_J|$, white color corresponds to $g_J = 0$. The density plots shown in (a)–(e) correspond, respectively, to the density currents $j = 0.33,0.37,0.47,0.57,0.77\,j_0$. Parameters of the system are discussed in the text.

of the sample. Those channels appear to be almost static. However, there are smaller isolated phase-texture islands between the channels that still travel from one side of the sample to the other. For larger currents the weaker band $j = 2$ gradually stops to be superconductive, starting from the upper boundary with the largest concentration of vortices. One sees this in Fig. 1(e), where the absence of the condensate results in $g_J = 0$ (white) in the upper part of the sample.

Further details of the formation of the phase textures and their relation to the process of vortex splitting are shown in Fig. 2, which plots a scaled part of the g_J density plot superimposed by the vortex structure in the bands. The latter are illustrated by the contour lines of the condensate density $|\psi_j|^2$. Vortices in the stronger band (smaller ξ_1) are represented by the black lines, while the vortices in the weak band (larger ξ_2) are given by magenta lines. Figures 1(a)–1(d) and Figs. 2(a)–2(d) are calculated for the same parameters.

One can clearly see how in the vicinity of the boundary vortices of the weak band move faster than those in the strong band making vortices fractional. However, those fractional vortices quickly recombine and become composite after leaving the boundary vicinity. For a stronger current the vortex density increases and the recombination is delayed as shown in Fig. 2(b). Here some fractional vortices moving inside the sample arrange themselves in quasi-1D patterns with vortices

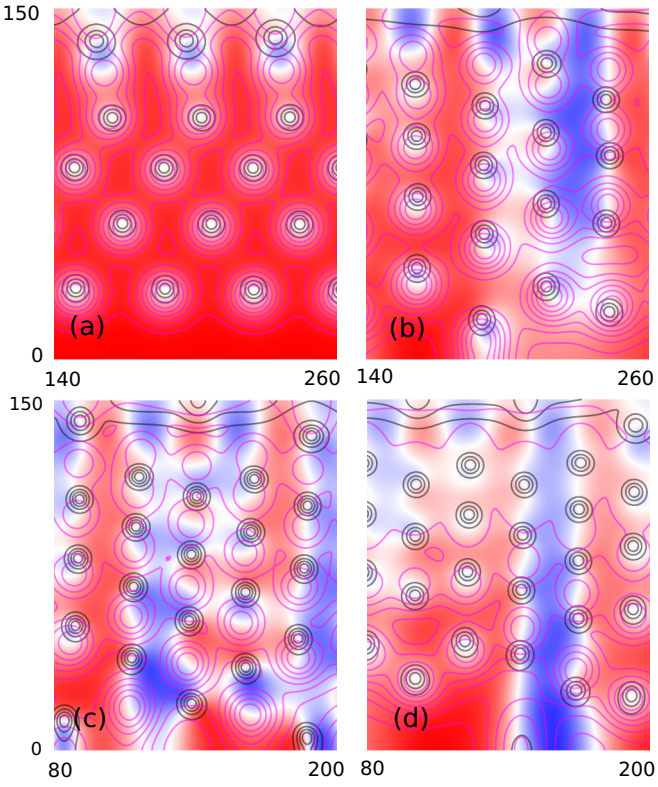

FIG. 2. Enlarged parts of the color density plots of g_J shown in Fig. 1, superimposed with the contour plots for the band condensate densities for the strong band $|\psi_1|$ (black line) and for the weak band $|\psi_2|$ (magenta line), which reflect the vortex structure in the band condensates.

in one band located opposite to vortices in the other band. In the middle of such 1D pattern there are domains of $g_J > 0$, which stretch towards the lower boundary. Vortices tend to be attracted to this domain and to recombine slower. If the current is not so large all vortices recombine when moving deeper inside the sample.

When the current increases further, the recombination is delayed even more and domains of $g_J > 0$ eventually reach the lower boundary, as in Figs. 2(c) and 2(d). Here the splitting of vortices that form the domains becomes complete: vortices are separated by distances comparable or exceeding ξ_j. Finally, Fig. 2(d) also demonstrates how the condensate in the weaker band starts to disappear at the upper boundary, together with the vortex structure.

Figures 1 and 2 demonstrate that quasi-1D domains of the band phase shift is the result of the process where vortices split and arrange themselves in an alternating order, somewhat similar to antiferromagnetic spin ordering. This ordering is related to the balance between the vortex-vortex interactions, which is mainly attractive between vortices in different bands and is repulsive for vortices within the same band. The balance of the interactions depends on the band condensate densities and, therefore, on the current. When the current grows, the condensate is depleted and the repulsion, which is determined by the magnetic field distribution, gradually becomes dominant.

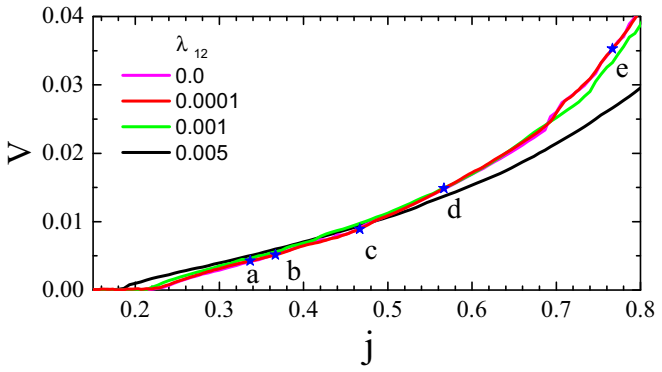

FIG. 3. I-V characteristics for the set of the interband couplings $\lambda_{12} = 0$, 0.0001, 0.001, and 0.005. Points a–e on the curve for $\lambda_{12} = 0.0001$ correspond to Figs. 1(a)–1(e) and Figs. 2(a)–2(c), respectively. Notice that the I-V characteristics for $\lambda_{12} = 0$ and 0.0001 are almost the same.

C. Current-voltage ($I-V$) characteristics

When vortices start to move their motion gives rise to energy dissipation and to the appearance of a finite voltage between the opposite sample boundaries in the direction of the current. This is illustrated in Fig. 3, which plots the current-voltage ($I-V$) characteristic of the considered sample for $\lambda_{12} = 0$, 0.0001, 0.001, and 0.005. While the first three values of the interband coupling correspond to the regime of the phase textures inside the superconductor, the last coupling does not favor vortex splitting inside the sample. Hence, one can check the effect of the phase textures on the dissipation. Notice that the points a–e in Fig. 3 (on the curve for $\lambda_{12} = 0.0001$) correspond, respectively, to Figs. 1(a)–1(e) and Figs. 2(a)–2(d).

From Fig. 3 one sees that the threshold current density (onset of the dissipation) practically does not change with λ_{12} in the phase-texture regime. It remains near $0.23\,j_0$ despite the interband coupling changes by orders of magnitude. However, when the vortex splitting and the related phase textures do not penetrate inside the superconducting sample, the threshold current density shifts down by about 20%, i.e., increasing the impact of the dissipation.

However, strikingly enough, one cannot say generally that the dissipation is less pronounced for the couplings related to the penetration of the phase textures. Indeed, at large current densities the curves for $\lambda_{12} = 0$, 0.0001, and 0.001 exhibit a higher voltage and higher differential resistance than that of the sample at $\lambda = 0.005$. We arrive at the conclusion that the penetration of the phase textures inside the superconductor has a rather complex effect on the dissipation. For relatively small current densities the dissipation is less significant in the phase-texture regime, with a larger threshold current density for the vortex motion. For large current densities one finds the opposite result, i.e., the dissipation of the energy is more pronounced for the interband couplings favoring the vortex splitting inside the sample.

As also noted above, when the current density is sufficiently large $j > 0.707\,j_0$ the superconductivity in the weak band is destroyed [cf. Fig. 1(e)]. Then the resistance increases still further (cf. point e in Fig. 3), because at such strong currents the repulsion between vortices of the remaining condensate

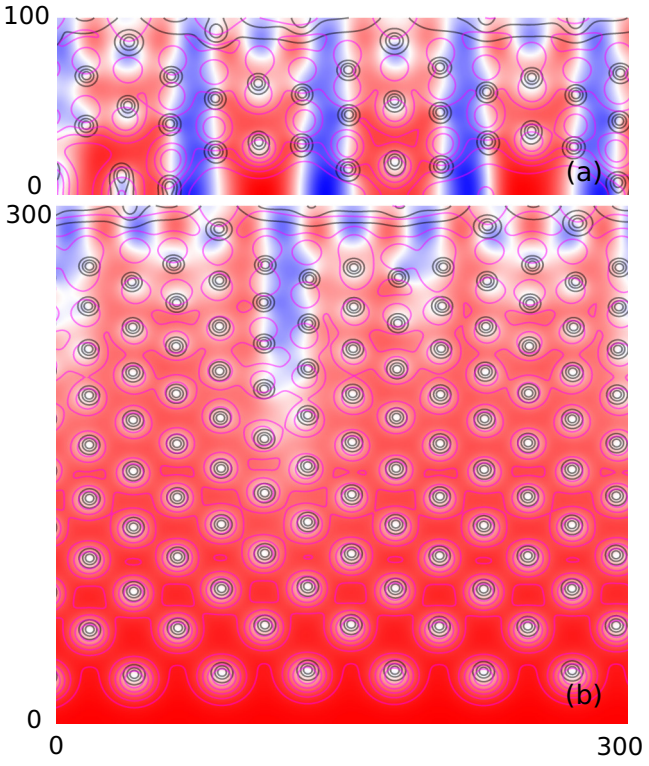

FIG. 4. Snapshots of the Josephson energy distributions calculated for the slabs with $L \times w = 600\xi_1 \times 100\xi_1$ (a) and with $L \times w = 600\xi_1 \times 300\xi_1$ (b). The contours represent the condensate density $|\psi_1|$ (black lines) and $|\psi_2|$ (magenta lines). The current is $j = 0.447 j_0$, other parameters are the same as in Figs. 1–3.

weakens and its vortices form a fluid instead of a rigid lattice. In the fluid the mobility of vortices increases considerably, leading to an increase in the resistance.

D. Size effects

As is shown above, the splitting of vortices which induces interband phase textures is related to the vortex-boundary interactions. One concludes that these as well as other phenomena, related to the splitting of vortices, strongly depend on the system size. In order to illustrate this dependence we consider dynamics of vortices in slabs of different sizes.

The results are illustrated in Fig. 4, which shows snapshots of the Josephson energy for the slabs with the same $L = 600\xi_1$ and two different $w = 100\xi_1$, shown in Fig. 4(a), and $w = 300\xi_1$, shown in Fig. 4(b). Other parameters of the system are the same as in Fig. 1. Figure 4 also shows contour plots for the spatial distribution of the band condensates $|\psi_j|$, as in Fig. 2.

The value of the current is taken as $j = 0.447 j_0$. For the smaller slab this current corresponds to a situation where split vortices form perpendicular phase textures with $g_J > 0$ [cf. Fig. 4(a)] that already connect the upper and the lower boundaries. However, for the larger slab the vortex distribution and g_J change, as shown in Fig. 4(b). Vortices that move towards the lower boundary gradually recombine so that deep inside the sample only composite vortices are found. For the chosen parameters the condensate in the weak band is suppressed when the current further increases. We cannot comment on the situation of full decoupling of vortices in high current as reported in Ref. [22]. This deserves special investigation, and results will be reported elsewhere.

IV. SUMMARY

This work investigates the mechanism of the formation of phase textures in 2D two-band superconductors, placed in the magnetic field. In comparison with equilibrium vortex distribution, the dynamic vortex matter demonstrates a number of specific properties, in particular vortex splitting. Composite vortices split spatially and create fractional vortices, each carrying a noninteger part of the unit quantum flux. The interaction between fractional vortices is a complex pattern, being repulsive for vortices within the same band and attractive for those in different bands. This interaction is responsible for arranging vortices in nonequilibrium alternating patterns, which helps to create quasi-1D phase textures or domains with the changed phase difference between the band condensates. This mechanism for the formation of the interband phase textures, induced by the vortex splitting, differs from that considered previously. We have shown that such phase textures have a significant effect on the dissipation caused by the vortex motion, which deserves further investigation.

ACKNOWLEDGMENTS

This work was supported by the Brazilian agencies Coordenação de Aperfeiçoamento de Pessoal de Nível Superior (CAPES) (Grants No. 223038.003145/2011-00 and No. 400510/2014-6), Conselho Nacional de Desenvolvimento Científico e Tecnológico (CNPq) (Grants No. 307552/2012-8 and No. 141911/2012-3), and Fundação de Amparo à Ciência e Tecnologia de Pernambuco (FACEPE) (APQ-0936-1.05/15).

[1] A. J. Leggett, Prog. Theor. Phys. **36**, 901 (1966).
[2] P. C. Canfield and G. W. Crabtree, Phys. Today **56**, 34 (2003).
[3] J. Paglione and R. L. Greene, Nat. Phys. **6**, 645 (2010).
[4] Y. Lubashevsky, E. Lahoud, K. Chashka, D. Podolsky, and A. Kanigel, Nat. Phys. **8**, 309 (2012).
[5] M. Zehetmayer, Supercond. Sci. Technol. **26**, 043001 (2013).
[6] G. Blumberg, A. Mialitsin, B. S. Dennis, M. V. Klein, N. D. Zhigadlo, and J. Karpinski, Phys. Rev. Lett. **99**, 227002 (2007).
[7] V. Stanev and Z. Tešanović, Phys. Rev. B **81**, 134522 (2010).
[8] J. Garaud, J. Carlström, and E. Babaev, Phys. Rev. Lett. **107**, 197001 (2011).
[9] S.-Z. Lin and X. Hu, New J. Phys. **14**, 063021 (2012).
[10] J. Garaud and E. Babaev, Phys. Rev. Lett. **112**, 017003 (2014).
[11] X. Hu and Z. Wang, Phys. Rev. B **85**, 064516 (2012).
[12] Z. Huang and X. Hu, Phys. Rev. B **92**, 214516 (2015).
[13] Y. Tanaka, Phys. Rev. Lett. **88**, 017002 (2001).

[14] A. Gurevich and V. M. Vinokur, Phys. Rev. Lett. **90**, 047004 (2003).
[15] S.-Z. Lin, J. Phys.: Condens. Matter **26**, 493202 (2014).
[16] E. Babaev, Phys. Rev. Lett. **89**, 067001 (2002).
[17] L. F. Chibotaru, V. H. Dao, and A. Ceulemans, Europhys. Lett. **78**, 47001 (2007); L. F. Chibotaru and V. H. Dao, Phys. Rev. B **81**, 020502(R) (2010).
[18] R. Geurts, M. V. Milošević, and F. M. Peeters, Phys. Rev. B **81**, 214514 (2010).
[19] J. C. Piña, C. C. de Souza Silva, and M. V. Milošević, Phys. Rev. B **86**, 024512 (2012).
[20] M. A. Silaev, Phys. Rev. B **83**, 144519 (2011).
[21] R. M. da Silva, M. V. Milošević, D. Domínguez, F. M. Peeters, and J. Albino Aguiar, Appl. Phys. Lett. **105**, 232601 (2014).
[22] S.-Z. Lin and L. N. Bulaevskii, Phys. Rev. Lett. **110**, 087003 (2013).
[23] Y. Matsunaga, M. Ichioka, and K. Machida, Phys. Rev. B **70**, 100502(R) (2004).
[24] M. E. Zhitomirsky and V. H. Dao, Phys. Rev. B **69**, 054508 (2004).
[25] A. Chaves, L. Komendová, M. V. Milošević, J. S. Andrade, G. A. Farias, and F. M. Peeters, Phys. Rev. B **83**, 214523 (2011).
[26] R. M. da Silva, M. V. Milošević, A. A. Shanenko, F. M. Peeters, and J. Albino Aguiar, Sci. Rep. **5**, 12695 (2015).
[27] V. G. Kogan and J. Schmalian, Phys. Rev. B **83**, 054515 (2011).
[28] W. D. Gropp, H. G. Kaper, G. K. Leaf, D. M. Levine, M. Palumbo, and V. M. Vinokur, J. Comput. Phys. **123**, 254 (1996).
[29] M. V. Milošević and R. Geurts, Physica C (Amsterdam) **470**, 791 (2010).
[30] C. P. Bean and J. D. Livingston, Phys. Rev. Lett. **12**, 14 (1964).